XMM-Newton CCF Release Note

XMM-CCF-REL-286

Astrometry: time-dependent boresight

A. Talavera, P. Rodríguez-Pascual, & M.Guainazzi

May 31, 2012

1 CCF components

Name of CCF	VALDATE	List of Blocks changed	CAL VERSION	XSCS flag
XMM_BORESIGHT_0022	2000-01-01T00:00:00	BORESIGHT OM_ANGVAR EMOS1_ANGVAR EMOS2_ANGVAR EPN_ANGVAR		No

2 Changes

The CCF described in this Release Note implements for the first time a new concept: the *time-dependent boresight*.

It has been shown that the Star Tracker and instrument axes alignment exhibits seasonal dependencies of unknown origin. While their exact pattern depends on the camera and the coordinate system, they can be broadly characterised as a seasonal pattern superposed to a long-term trend. Similar behaviours are seen when correlating the misalignment against other quantities (such as the astronomical position angle, or the source R.A.) with a seasonal dependence. Attempts at correlating the EPIC mis-alignments with housekeeping parameters monitoring the thermal state of the optics have yielded only inconclusive results so far.

The time dependency of the misalignment can be empirically modelled by means of a long term variation plus a periodic (nearly one year) oscillation (Talavera & Rodríguez-Pascual 2011):

$$\Delta = (P_1 + P_2 \times T + P_3 \times T^2) + P_4 \times \cos[2\pi(T - P_5)/P_6)]$$

where Δ is the measured offset, and T is the time in Julian days elapsed since January 1 2000. The offset are measured in celestial coordinates (R.A., Dec.), and converted into spacecraft coordinates

prior to fitting. The best-fit parameters are given in Tab. 1. The mis-alignments calculated through

Table 1: Best-fit parameters implemented in this CCF

Instrument/coordinate	P_1	P_2	P_3	P_4	P_5	P_6
EPIC/Y	0.32	3.0×10^{-4}	7.0×10^{-8}	-0.08	65	374.6
EPIC/Z	0.05	7.4×10^{-4}	1.5×10^{-7}	1.22	-0.5	362.1
OM/X	-1.53	9.8×10^{-4}	-1.0×10^{-7}	-1.15	5.8	361.6
OM/Y	-2.64	2.4×10^{-3}	-2.8×10^{-7}	0.84	-4.7	362.4

the above formula are sampled in intervals of 5 days, are translated into increments applied to the Φ and Θ Euler angles. The extensions of this CCF include tables with the increments for each instrument as a function of the Modified Julian Date.

In this CCF version, the increment values are the same for all EPIC cameras (this solution yields a statistically more accurate position reconstruction with respect to using independent increments applied to each camera due to the statistical quality of the calibration sample). No calibration is currently available for the effect of these mis-alignments on the RGS wavelength scale.

3 Scientific Impact of this Update

The XMM-Newton astrometry is expected to significantly improve with this CCF. As shown in Sect. 6, the offsets between coordinates of XMM-Newton detected sources, prior to any rectification against an astrometric reference catalogue, and those of catalogue matches are considerably reduced after the application of the "time-dependent boresight". Furthermore, for cases where cross identification is not possible, the empirical correction implemented in this CCF ensures that the errors in the XMM-Newton coordinates are smaller.

4 Estimated Scientific Quality

The quality of the corrections can be assessed by comparing the position of astronomical sources detected by XMM-Newton against those of matching sources in optical catalogues when the old "constant" and the new "time-dependent boresight" are used to process the data.

5 Test procedures

Testing of the new CCF and the corresponding new CAL routines to access the new structure has been accomplished by running SASv12 (in the development track) on over 4000 ODFs covering the whole XMM-Newton operational life. Data were processed through standard SAS tasks

(`e[mp]proc/omichain`). For both instruments USNO has been the reference catalogue (as used by, *e.g.*, the SAS `eposcorr` task).

6 Summary of the test results

6.1 EPIC

In Fig. 1 we show the offset in celestial (R.A. and Dec) and spacecraft coordinate (Y/Z) space as a function of time when the "constant" (*left columns*) and the "time-dependent" (*right column*) boresight are used. Visual inspection suggests that any time-dependent trend is efficiently removed. In Fig. 2 histograms of the same quantities are shown. The main improvement in the coordinate accuracy is along the Z spacecraft direction. The average offset $\langle\Delta\rangle_Z$ goes from $\simeq$-0.6 to $\simeq$0.1 arcseconds. The width of the distribution improves as well (from $\simeq$1.5 to $\simeq$1.2 arcseconds). The improvement along the spacecraft Y axis is, instead, negligible.

6.2 Optical and UV Monitor (OM)

Cross-correlations with USNO Catalogue are performed with SAS during pipeline processing and stored in the XSA. We have retrieved data from about 4500 observations and we have reprocessed these same data using the new variable boresight.

From XSA data (`OBSMLI` files) processed with the "standard" boresight, we obtain average offsets of -0.36 and 0.56 arcseconds in R.A. and Dec., respectively. The standard deviations of these offsets are 1.6 and 2.0 arcseconds.

Using the new boresight in the cross-correlations reduces these errors to average offsets of -0.12 and 0.26 arcseconds with standard deviations of 1.2 and 1.1 arcseconds in R.A. and Dec., respectively.

Fig. 3 summarises the test results and shows clearly the improvements obtained with the time-dependent boresight. In the *left hand side panels* we show the offsets against the USNO B1 catalogue obtained from the XSA. In the *right hand side panels* we show the new values obtained with the new method.

The most striking effect was seen when converting the R.A. and Dec. offsets to their equivalent X and Y in the OM focal plane. This conversion uses the Position Angle of the observations. In the *lower panels* of Fig. 3 we see the comparison in X and Y. The long term and the periodic variation disappear when using the time-dependent boresight. Also the mean and sigma values decrease considerably.

Another effect of the misalignment present in the current, constant boresight is the dependency of the offsets measured in R.A./Dec. with the Position angle. Fig. 4 shows this dependency and how it disappears. We represent the offsets of 250 observations obtained in 2009. We see in the

upper panels a bimodal distribution in R.A./Dec. and a clear offset from zero in X/Y. Both effects disappear with the new time-dependent boresight (*lower panels*). The same effect, but for the more than 4000 observations of Fig. 3 is presented in Fig. 5. The R.A./Dec. comparison is in the *upper panels*, and the X/Y in the *lower panels*.

7 Expected updates

The long term trend seen in the OM X/Y offsets (Fig. 3) seems to be reaching a plateau.

We need to monitor the offsets in the future to confirm the trend or to modify the fit to that trend into the CCF. We are confident that the new CCF will be valid at least until the end of 2012. Updates will follow accordingly.

Efforts are still ongoing to discover the physical driver(s) of these time-dependent effects, with the ultimate goal of replacing the empirical description embedded in this CCF with a physically-motivated law.

References

Talavera A., Rodrìguez-Pascual P., 2011, XMM-SOC-TN-0041, available at:
`http://xmm2.esac.esa.int/x̃mmdoc/CoCo/CCB/DOC/Attachments/INST-TN-0041-1-0.pdf`.

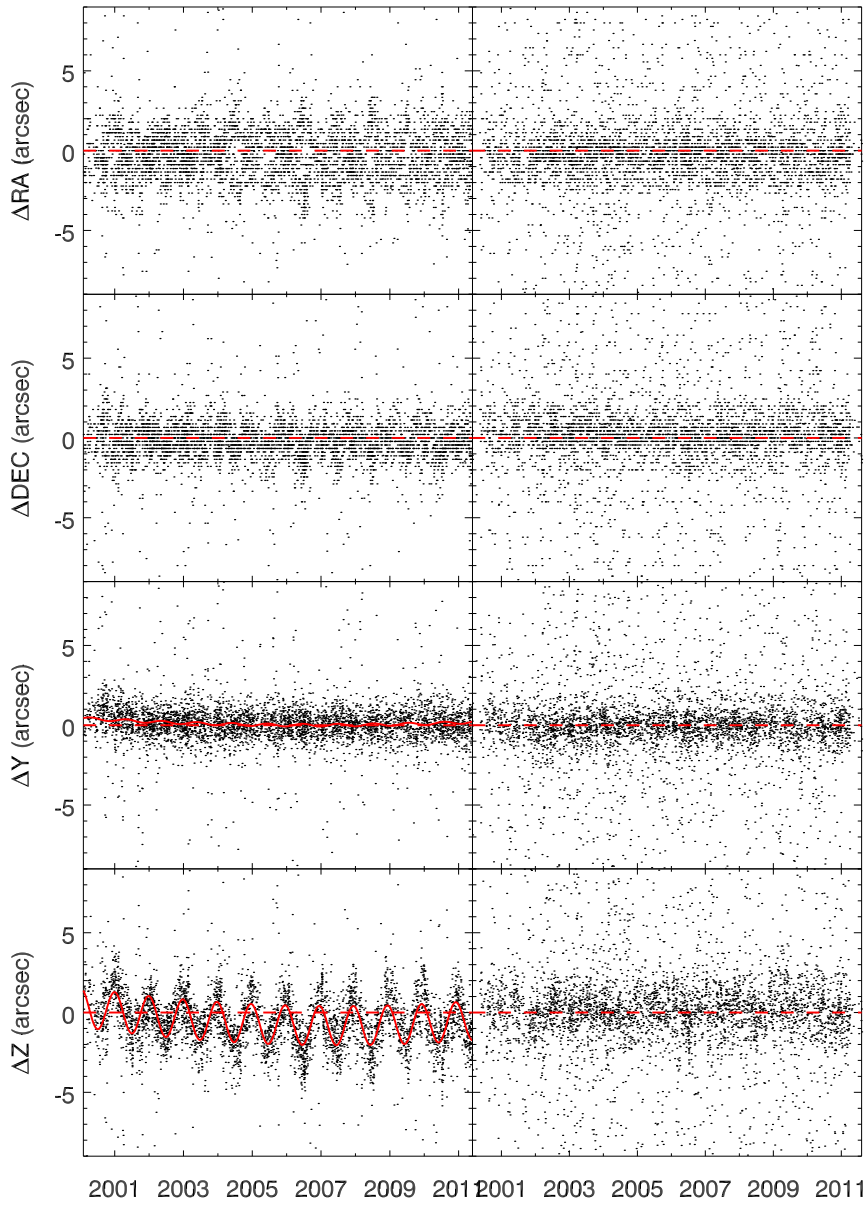

Figure 1: EPIC positional offsets in celestial and spacecraft coordinates (from *top* to *bottom*: ΔR.A, ΔDec., ΔY and ΔZ) as a function of time (years) for the "constant" (*left column*) and the "time-dependent" (*right column*) boresight. The *dashed red lines* indicate the 0 level; the *solid red lines* in the ΔY/ΔZ panel of the *left column* indicate the linear best-fit.

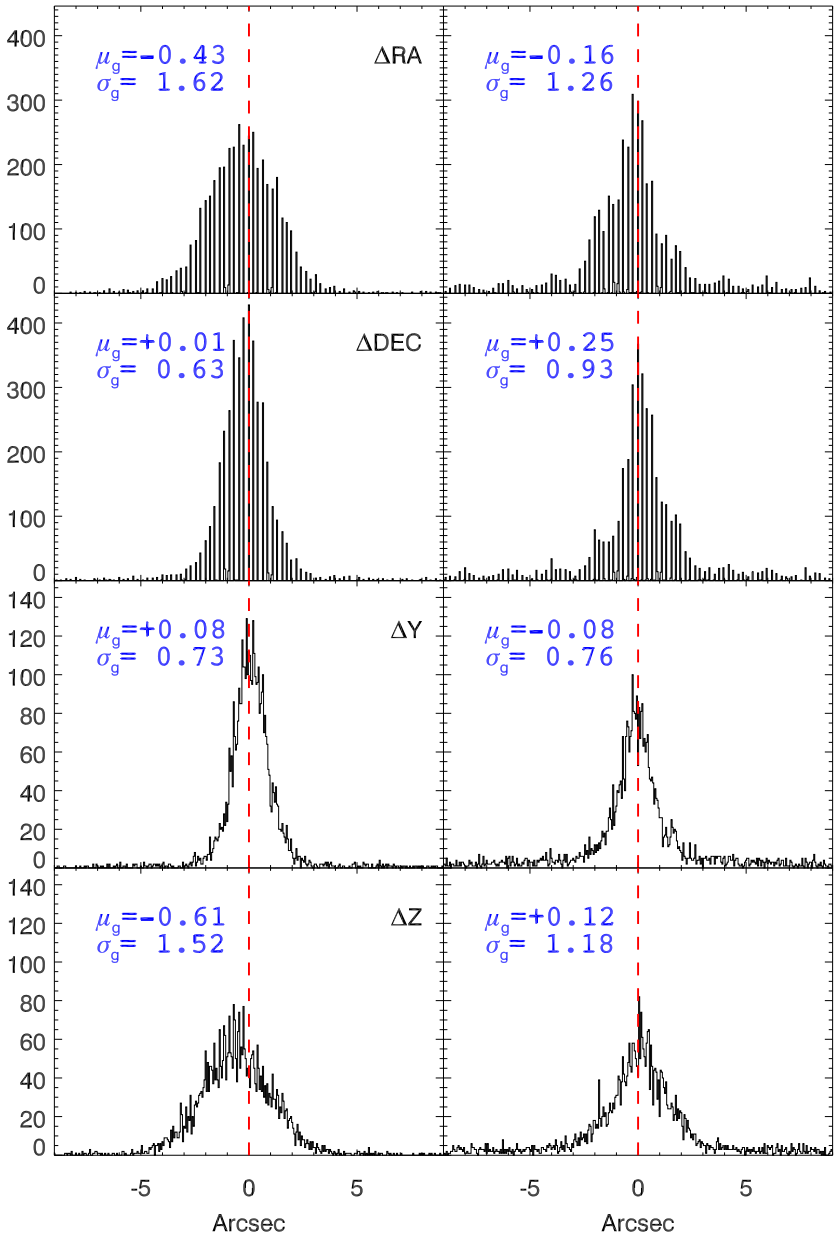

Figure 2: Histogram of the EPIC positional offsets in celestial and spacecraft coordinates (from *top* to *bottom*: ΔR.A, ΔDec., ΔY and ΔZ) for the "constant" (*left column*) and the "time-dependent" (*right column*) boresight.

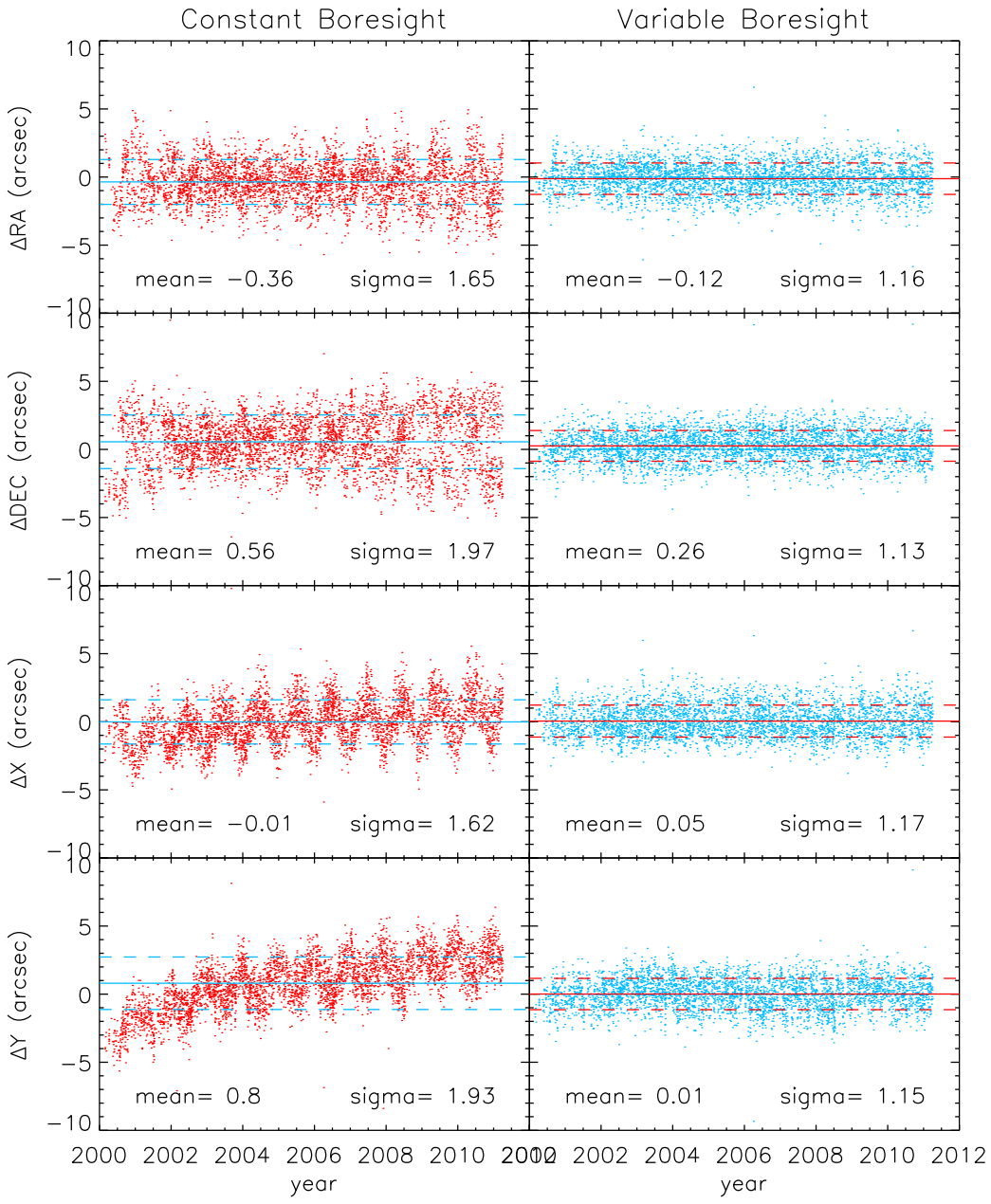

Figure 3: OM positional offsets against the USNO catalogue using "constant" (*left panels* and the new "time-dependent" boresight (*right panel*.

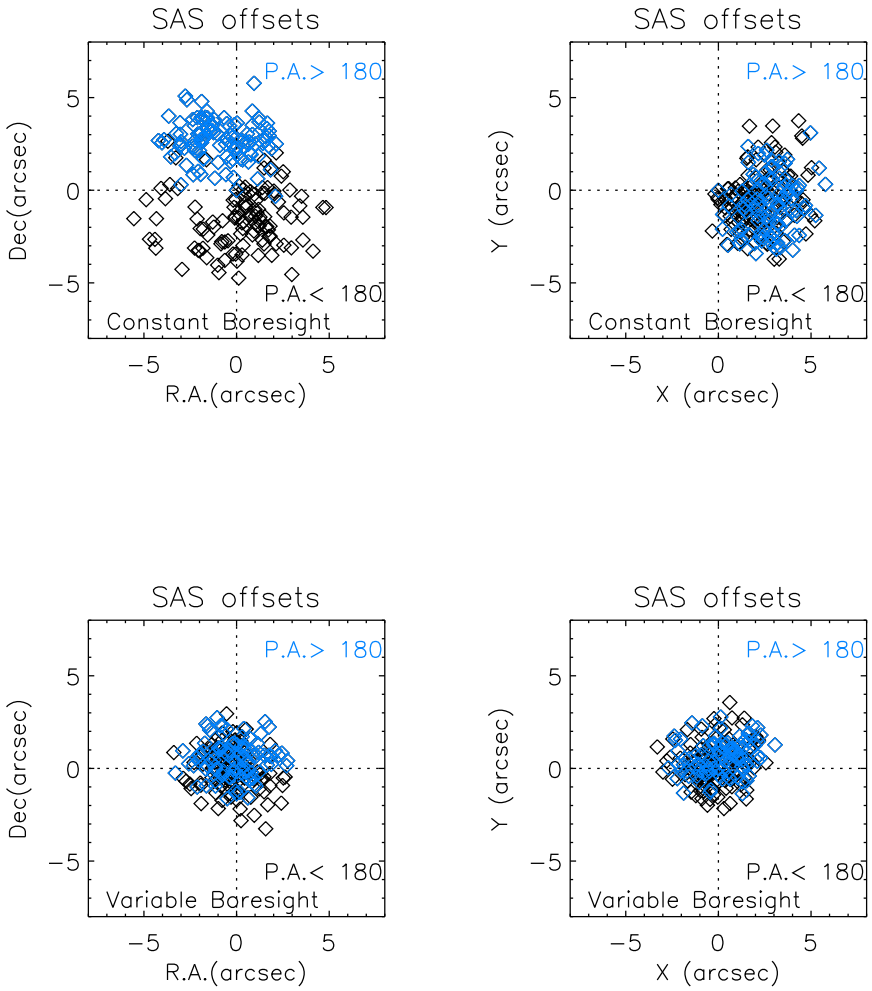

Figure 4: Effect of the Position Angle on the OM positional offsets for a sample of observations performed in 2009.

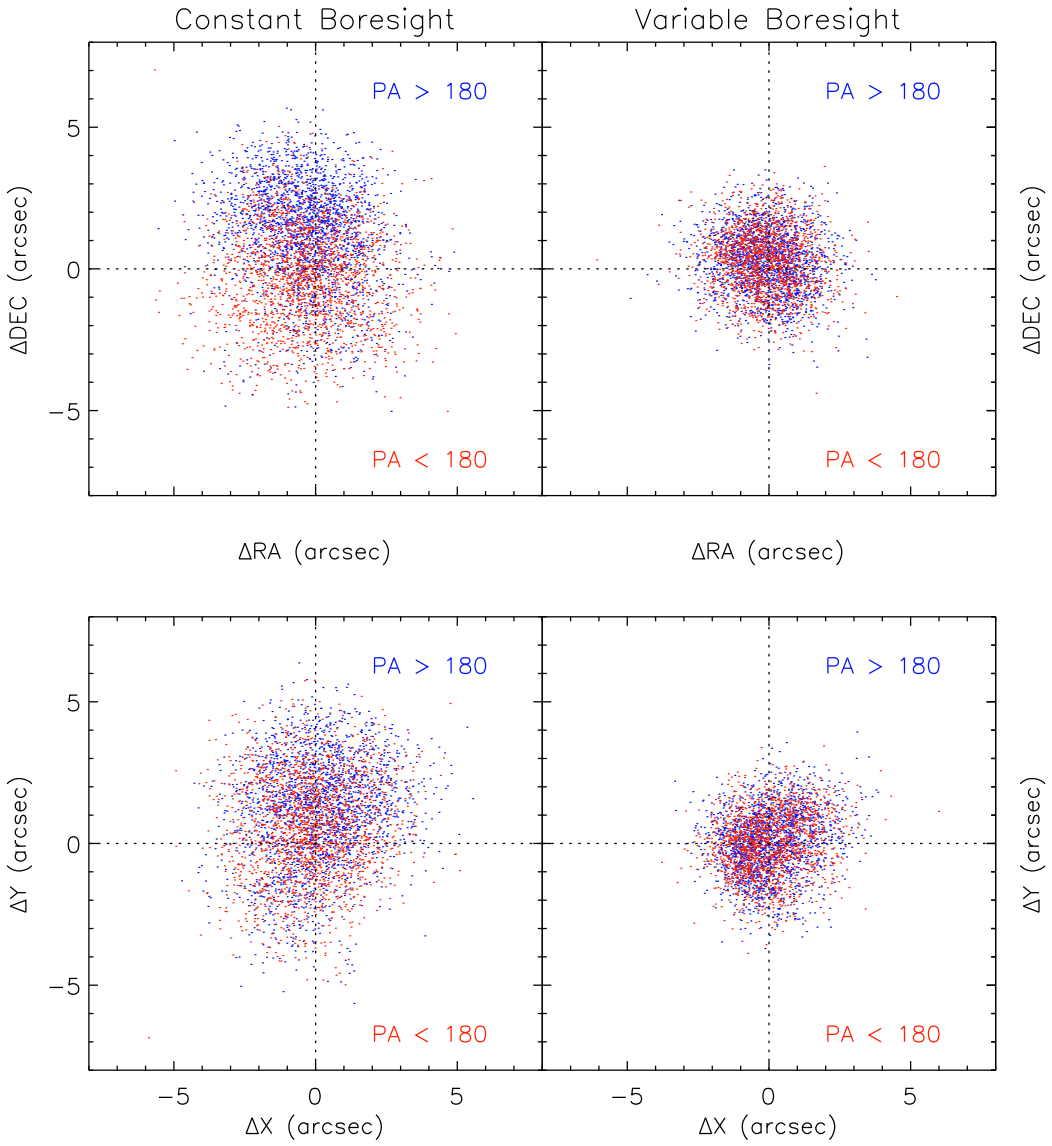

Figure 5: Effect of the Position Angle for all observations of Fig. 3.